Examination of the Proper Orthogonal Decomposition and Correlation Function of the Turbulent Flow at the Aft of a Body of Revolution at Inclination

Jarrod T. Banks *, William J. Devenport †
Virginia Tech, Blacksburg, VA, 24060

The proper orthogonal decomposition and the correlation structure of a turbulent profile on the port side at the aft of a body of revolution inclined at five degrees angle of attack was investigated. Measurements were taken at a body diameter based Reynolds number of 600,000 and a rotor advance ratio of J=1.27. Particle image velocimetry was taken at two principal locations on the lee and port side at the aft of the body. The turbulent modes were dominated by the embedded shear layer and both u_x and u_r modal profiles appeared similar in form. The spatial correlations show fairly narrow, high magnitude, auto-correlations while the cross-correlations extend over a larger separation distance with a lower relative magnitude. Similar trends were noted for the temporal correlations except the auto-correlations extended well into the time domain. All correlations peaked in the embedded shear layer.

Nomenclature

a	=	random time coefficient
D	=	body of revolution diameter
f_s	=	sampling frequency
Hz	=	unit of frequency
m	=	meters
mm	=	millimeters
m/s	=	meters per second
n	=	Mode number
R_{ij}	=	correlation function
$\overline{U}$	=	mean velocity (m/s)
u_i	=	fluctuating velocity (m/s)
^{o}	=	degrees

*Graduate Researcher, Department of Aerospace and Ocean Engineering and AIAA Student
†Crofton Professor of Engineering, Center for Research in Experimental Aero/Hydrodynamic Technology, Fellow AIAA

λ = eigenvalue

τ = time delay (s)

ϕ = eigenvector

Subscripts

i, j, k = direction subscripts

x, r, θ = body defined coordinate system

I. Introduction

In many flows of interest rotors interact with some form of turbulence. The interaction between the rotor and the flow produces sound from the velocity fluctuations interacting with the rotor. While turbulence is inherently stochastic or random in nature there are often coherent eddies that can be identified in many turbulent flows. These eddies can vary both in time and space and many reduced order analyses depict the eddies as only a spatial distribution. However, using Taylor's frozen flow hypothesis, the time correlations can be stretched into the spatial domain using a convection velocity. Ultimately, in the application of rotor turbulence ingestion noise, the rotor is a time varying sampler of the flow and is far more concerned with the temporal evolution of an eddy rather than what it strictly appears as in the spatial domain. Devenport et al. [1] and Glegg and Devenport [2] demonstrated a compact method to represent instantaneous eddies responsible for the production of sound from an airfoil. This method is referred to as Compact Eddy Structures (CES) and takes the Proper Orthogonal Decomposition (POD) of the turbulence in the inhomogenous directions and extends each mode in the homogenous directions using a linear multiplication between the mode and the time correlation function.

In this paper the POD of the turbulent flow and correlation function about a body of revolution at an angle of attack will be presented. In Section II the reduced order methods of POD, LSE, and CES will be described and the method of application shown. The following Section III will describe the experimental setup. Section IV will begin with a view of the instantaneous velocity followed by a characterization of the mean velocity and Reynolds stress, then the POD modes, and the spatio-temporal correlation function for a profile just upstream of the rotor.

II. Flow Decomposition

A. Proper Orthogonal Decomposition

Proper Orthogonal Decomposition is a form of reduced order analysis and derives its use from a Principal Component Analysis known as a Karhunen-Loeve decomposition. This decomposition, like so many of the techniques used when examining turbulent velocity fields, finds its roots in statistics. It was first used in the context of turbulence and coherent eddy identification by Lumley [3]. It aims to find a basis for a modal decomposition from a space or time based signal ensemble by solving the Fredholm equation and is simply the eigenvalue decomposition of the zero time-delay correlation function R_{ij},

$$\int R_{ij}(x, r, x', r', 0)\phi_j^{(n)}(r')dz' = \lambda^{(n)}\phi_i^{(n)}(r) \quad (1)$$

This allows the flow to be described by a certain number of orthonormal modes, ordered by energy contribution to the overall mean square of the velocity fluctuations. The eigenvalues, represented by $\lambda^{(n)}$ in equation 1, give the modal energy, while the eigenvectors, represented by $\phi_i^{(n)}(r)$, give the velocity distribution at a point r. The velocity field can then be reconstructed at each mode using the time coefficients in the following manner,

$$u_i(r, t) = \sum_n a_n(t)\phi_i^{(n)}(r) \quad (2)$$

In homogenous turbulence POD reduces to the more familiar Fourier decomposition in wavenumber space and is less useful in the reconstruction of flow eddies. In an

effort to recreate the most probable instantaneous eddies a combination of POD and a statistical method known as Linear Stochastic Estimation (LSE) will be used. The details of LSE and a mathematical extension termed Compact Eddy Structures (CES) will be described in the next section.

B. Linear Stochastic Estimation and Compact Eddy Structures

Linear stochastic estimation is a method of producing eddy like structures within a flow. Given some initial condition, such as a starting velocity fluctuation, the variation of this velocity with either time or space can be readily determined through a linear multiplication of the starting condition with the correlation function of the flow.

$$u_j(x', r' - r, \tau)|_{LSE} = R_{ij}(r, r', r' - r, \tau) \left[u_i(r) / \overline{u_i(r)^2} \right] \tag{3}$$

This is most applicable to homogenous turbulence, while POD is most efficient in application to inhomogenous turbulence. Thus we can apply POD in the inhomogenous directions of a turbulent flow to obtain the most energetic modes while using the simpler linear stochastic estimation in the homogenous directions and obtain eddy like structures. This method is referred to as Compact Eddy Structures and will be applied in the following section. The CES of a flow can be given by summing up all contributions to each flow from the correlation function at each point,

$$u_j^{(n)}(r', x' - x, \tau)|_{CES} = \frac{1}{\lambda^{(n)}} \int \phi_i^{(r)} R_{ij}(r, r', x' - x, \tau) dr \tag{4}$$

This method is useful as it only requires a small fraction of the data as an input to compute much of the turbulent flow the rotor experiences. It requires a sufficiently long time series for the statistics to be converged but it is still relatively memory compact as it only requires a profile just upstream of the rotor inflow to describe much of the flow field the rotor interacts with.

C. Flow Application

We will begin by writing the fluctuating velocity time series for a one dimensional profile $u_i(x, r, t)$ and then decompose the flow using POD in the inhomogenous direction, given by r, for a single profile at the rotor inlet, $x/D = 3.17$. This is done by solving equation 1. The correlation function that will be used to extend the POD profiles into the time domain is calculated for the profile at zero time delay (spatial profile correlation) and zero separation (temporal profile correlation). Application of the correlation function to compute the compact eddy structure is left for a separate paper.

III. Experimental Methods

A. Experimental Facility

Experimental measurements of the body of revolution (BOR) were made in the Virginia Tech Stability Wind Tunnel (VTSWT) in its' anechoic configuration. The test section consists of two Kevlar side walls and a floor and ceiling formed from Kevlar covered panels treated to minimize acoustic reflection. It has dimensions of 1.85 m x 1.85 m x 7.32 m and flow is generated using a 5 bladed, 4.3 m diameter fan. Maximum flow capability of this facility is 80 m/s with freestream turbulence levels less than 0.01% at 20 m/s and a freestream uniformity of 0.5% at 47 m/s

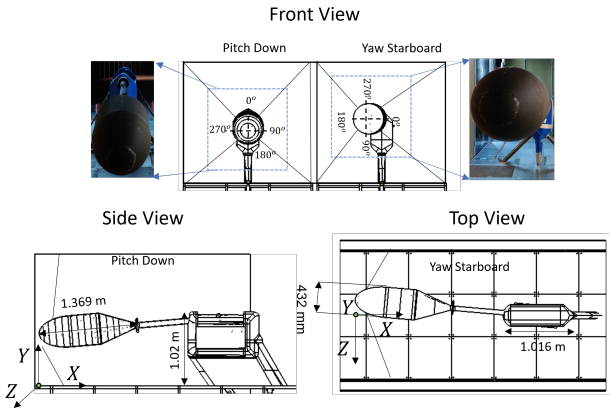

Fig. 1 Schematic of the experimental setups used to measure different sections of the flow about the body. The top row shows the front view of the pitch down and yaw starboard configurations. The bottom row shows the side of the pitch down configuration and the top view of the yaw starboard configuration. Principal dimensions of the body and structure are shown as well as the approximate location of the tethers.

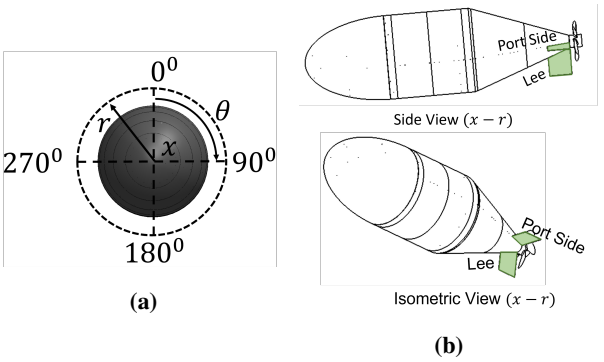

Fig. 2 a) Body centered cylindrical coordinate system with the x coordinate positive axially downstream, r-coordinate positive normal to the body surface, and θ coordinate positive clockwise. The streamwise coordinate x is perpendicular to the $r-\theta$ plane and the rotor rotates anti-clockwise in this frame of reference. b) Schematic showing the side and isometric views of the location of the PIV measurements in the $x-r$ plane.

(Devenport et al. [4]) . Figure 1 shows the two orientations of the body of revolution as tested.

B. Model

The BOR was tested in two configurations; pitch down and yaw starboard. The nose is a 2:1 ellipsoid and the midbody is a 432 mm diameter cylinder, and the aft section is a 1.17D long section with a 20^o ramp that produces an adverse pressure gradient. Trip rings at $x/D = 0.98$ produce a turbulent boundary layer which is grown over the length of the midbody. A tether system consisting of four 1.58mm diameter wires were used to anchor the cantilevered body of revolution in place. The tethers are attached at $x/D = 1$ and extend to the corners of the test section. The rotor blades are a modified NACA 66 airfoil made from 6061 aluminum and the 216 mm diameter rotor is mounted on a 50 mm diameter drive shaft.

C. Body Centered Coordinate System

The local coordinate system used for the BOR in the experimental test is a right-handed, body oriented cylindrical system shown in Figure 2a. The origin is centered on the BOR nose and the principal coordinates are described looking at the BOR nose from upstream. x is positive downstream along the body axis, r is always positive and radiates outward orthogonal to the x coordinate, and θ is referenced orthogonal to the x coordinate and in the same plane as the radial component. θ is positive clockwise when viewing the nose from upstream. To aid in discussion of the various parts of the flow the location of each measurement plane will be defined in the context of Figure 2. The body centered coordinates are oriented such that $\theta = 180^o$ corresponds to the lee side. Conversely, the windward side occurs at $\theta = 0^o$ and the port and starboard sides of the body are at $\theta = 90^o$ and 270^o respectively.

D. Particle Image Velocimetry

The velocity and turbulence at the aft of the BOR was measured using particle image velocimetry (PIV). The imaged region extended over a 160 x 160 mm^2 area with a 4.2 mm spatial resolution. A Photonics Industries DM laser combined with two Phantom v2512 cameras equipped with Nikon 200 mm lenses and a Davis PTU X timing unit were used to acquire the PIV. The sampling rate used was 12.848 kHz and the cameras acquired data in dual frame/dual pulse mode. The PIV was recorded in blocks referred to as cycles that begin at the same point of the shaft rotation for each block of data. This was achieved using an optical sensor and a mark on the shaft that sent a trigger signal to the PTU once per rotation. This method of data acquisition allowed phase averaging of the velocity field and hence phase averaged subtraction of the mean velocities to give a truly zero mean velocity time series.

IV. Results and Discussion

We will start with a look at the instantaneous and mean velocities for the two planes of interest. All data presented here was taken at a body diameter based Reynolds number of 600 000, and a rotor advance ratio of $J = 1.27$. Figure 3a and b show the contours of the instantaneous velocity for two planes taken at the body. Quite clearly the flow in figure 3b displays higher spatial variation while that in figure 3a is significantly smoother. This is manifested further in figure 4a and b where a band of high $\overline{U_x}$ variation with r/D is seen between $r/D = 0.25$ and $r/D = 0.18$. This corresponds to the location of a band of high Reynolds normal stress seen in figure 5b. Banks et al. [5] investigated and identified the source of this high turbulence region to be three dimensional separation as a result of a highly

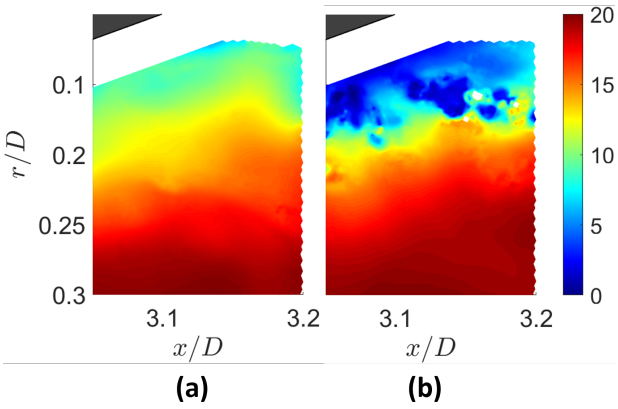

Fig. 3 Contours of the instantaneous axial velocity $\overline{U_x}$ (m/s) on (a) the lee ($\theta = 180^o$) and (b) the port ($\theta = 90^o$) side of the body of revolution.

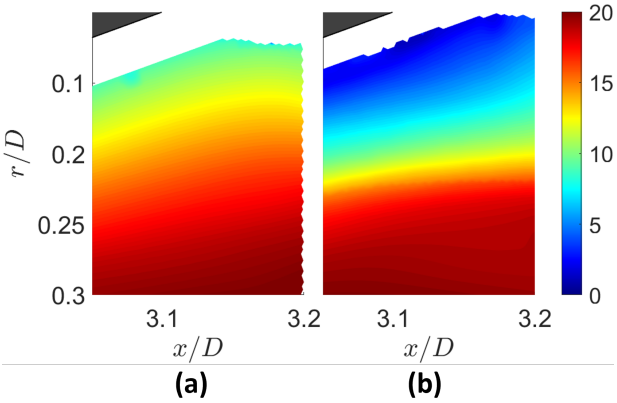

Fig. 4 Contours of the mean axial velocity $\overline{U_x}$ (m/s) on (a) the lee ($\theta = 180^o$) and (b) the port ($\theta = 90^o$) side of the body of revolution.

adverse pressure gradient on the lee side pulling near wall turbulence away from the wall. This separation then rolls up into a pair of vortices between the lee and body sides. A profile at $x/D = 3.17$ for the port side data will now be investigated and the zero time delay and zero separation correlation functions examined.

The correlation functions presented here are those used to extend the POD modal profiles into the homogenous directions and only presented for the port side PIV plane ($\theta = 90^o$). Figure 6 shows the zero time delay and zero spanwise separation correlation function for the profile at

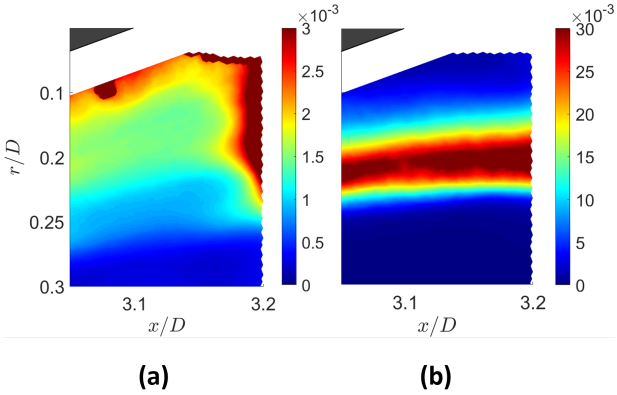

Fig. 5 Contours of the mean Reynolds normal stress normalized on the square of the free stream velocity $\overline{u_x^2}/U_\infty^2$ on (a) the lee ($\theta = 180^o$) and (b) the port ($\theta = 90^o$) side of the body of revolution.

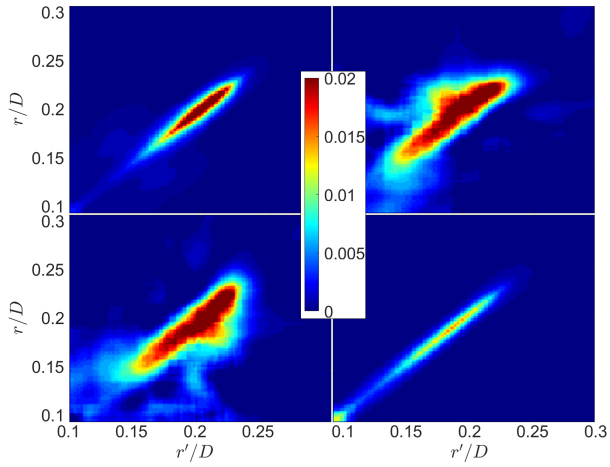

Fig. 6 The zero time delay and separation correlation function for a profile at $x/D = 3.17$. The correlation function is normalized on the square of the freestream velocity in the following way $R_{ij}(r/D, r/D', 0, 0)/U_\infty^2$. From top left to bottom right, $R_{u_x u_x}$, $R_{u_x u_r}$, $R_{u_r u_x}$, $R_{u_r u_r}$. The cross-correlation terms, $R_{u_x u_r}$ and $R_{u_r u_x}$ contours are plotted at 1/10th the contours shown on the colorbar.

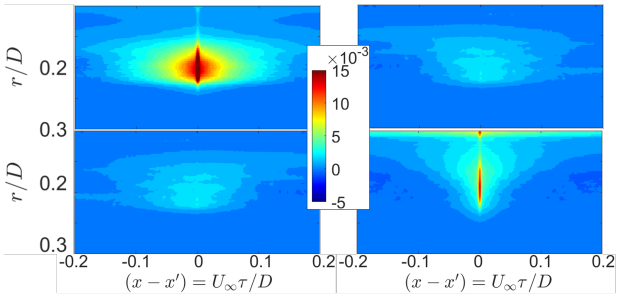

Fig. 7 The zero separation correlation function for each point in a profile at $x/D = 3.17$. The correlation function is normalized on the square of the free stream velocity in the following way $R_{ij}(r, 0, x - x', \tau)/U_\infty^2$. From top left to bottom right, $R_{u_x u_x}$, $R_{u_x u_r}$, $R_{u_r u_x}$, $R_{u_r u_r}$

$x/D = 3.17$. This is the correlation between each r/D point and every other point in the profile represented by r/D'. Clearly there will be a maximum auto-correlation (top left $R_{u_x u_x}$ and bottom right $R_{u_r u_r}$) when $r/D = r/D'$ as the correlation between the same point is, by definition, perfect. This is represented in the contours by the maximum for each profile occurring along the diagonal of the plot. For both autocorrelations there is a corresponding slightly negative correlation just outside of the main lobe. The correlation of the u_r fluctuations extends over a greater radius than the u_x fluctuations however the u_x has a greater separation correlation over the separation distance. That is to say, the width of the $R_{u_x u_x}$ lobe is greater than that of $R_{u_r u_r}$. The cross correlation terms (top right $R_{u_x u_r}$ and bottom left $R_{u_r u_x}$) extend further with separation distance than the auto-correlation terms however, it should be stated that the cross-correlation values are overall ten times lower than the auto-correlation values. This implies that the velocity fluctuations will be dominated by the auto-correlation terms in both the u and r directions when reconstructing the turbulent velocity field with the compact eddy structure formulation.

In figure 7 the zero separation, time delay correlation function is presented for each point in the profile. Each horizontal contour slice is an independent time series. The turbulent shear layer evident in figure 5 clearly appears in the high correlations for all components of $R_{ij}(0,0,x-x',\tau)$ around $r/D = 0.2 \pm 0.05$. Once again the cross-correlation terms extend over a larger separation distance than the auto-correlation terms but have significantly lower correlation values. This is best illustrated in figure 8 which shows a horizontal slice of figure 7 at $r/D = 0.2$. This slice demonstrated the dominance of the auto-correlations on the overall energy in the flow with a correlation value of $0.03U_\infty^2$ for the u_x auto-correlation and $0.015U_\infty^2$ for the u_r auto-correlation. Contrasting this to the cross-correlation terms which were approximately 1/10th of the auto-correlations.

The dominant modes of the proper orthogonal decomposition were computed using the eigenvector decomposition and are shown in figures 9 and 10. The first three modes were computed as they comprise 35% of the total energy in the flow. The first mode in figure 9 clearly shows the primary energy captured within the embedded shear layer and for the subsequent modes there is very little modal energy outside of the shear layer.

An extension of this analysis is to follow in a further paper and the compact eddy structure of the flow will be computed from the POD modes.

V. Conclusion

The decomposition of a turbulent profile using proper orthogonal decomposition and the examination of its spatial and temporal correlation functions was done for the flow at the aft of a body of revolution at angle of attack. This

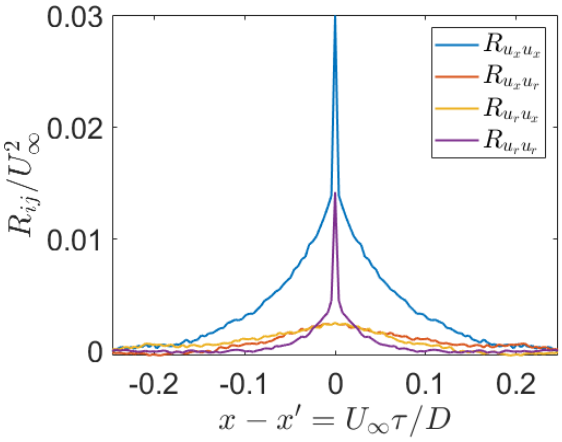

Fig. 8 Slice through the contour plot of $R_{ij}(r/D, 0, x - x', \tau)/U_\infty^2$ seen in figure 7 at r/D=0.2. Blue curve is the axial auto-correlation, purple curve is the radial auto-correlation and the yellow and orange curves are the cross-correlation terms between u_x and u_r.

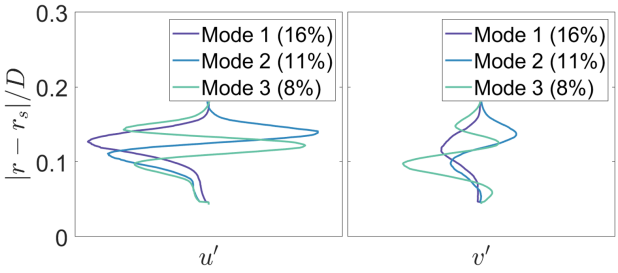

Fig. 9 Proper orthogonal decomposition for a profile at $x/D = 3.17$. Profiles are shown for the first three modes which comprise 35% of the total energy.

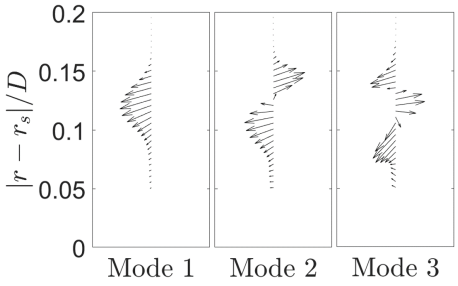

Fig. 10 Flow visualization of the modes produced from proper orthogonal decomposition of a profile at $x/D = 3.17$. The first three modes are shown from left to right.

revealed the impact of a high turbulence shear layer on the dominant fluctuating velocity modes. POD of the three most energetic modes demonstrated that the axial and radial fluctuations occur at roughly the same location in the profiles for each mode, and that these modes account for 35% of the total flow energy. Both the spatial and temporal parts of the correlation function demonstrate the dominance of the auto-correlation terms over the cross-correlation terms and will be the primary drivers of the eddy structure. An examination of the compact eddy structure will be done in a follow up paper.

Acknowledgments

The authors would like to thank the Office of Naval Research for sponsoring this work under grant N00014-20-1-2650, and specifically Drs. Yin Lu Young, Ki-Han Kim and John Muench. Further acknowledgements go to Humza Butt, Vidya Vishwanathan, Shishir Damani, Rachel Andrews, Aayush Salot, and Shivam Khullar amongst others for their assistance during the wind tunnel experiments. The author would also like to thank Mr. Michael Marcolini for his ever present advice.

References

[1] Devenport, W., Muthanna, C., Ma, R. L., and Glegg, S., "Two-Point Descriptions of Wake Turbulence with Application to Noise Prediction," *AIAA Journal*, Vol. 39, No. 12, 2001, pp. 2302–2307.

[2] Glegg, S. A. L., and Devenport, W. J., "Proper Orthogonal Decomposition of Turbulent Flows for Aeroacoustic and Hydroacoustic Applications," *Journal of Sound and Vibration*, Vol. 239, No. 4, 2001, pp. 767–784. https://doi.org/10.1006/jsvi.2000.3128.

[3] Berkooz, G., Holmes, P., , and Lumley, J. L., "The Proper Orthogonal Decomposition in the Analysis of Turbulent Flows," *Annual Review of Fluid Mechanics*, Vol. 25, No. 1, 1993, pp. 539–575. https://doi.org/10.1146/annurev.fl.25.010193.002543, URL http://www.annualreviews.org/doi/abs/10.1146/annurev.fl.25.010193.002543.

[4] Devenport, W. J., Burdisso, R. A., Borgoltz, A., Ravetta, P. A., Barone, M. F., Brown, K. A., and Morton, M. A., "The Kevlar-walled anechoic wind tunnel," *Journal of Sound and Vibration*, Vol. 332, No. 17, 2013, pp. 3971–3991. https://doi.org/10.1016/j.jsv.2013.02.043.

[5] Banks, J. T., Butt, H., Alexander, N., and Devenport, W., "Turbulence Ingestion of an Axisymmetric and Non-Axisymmetric Wake Into an Open Rotor," *Journal of Fluid Mechanics*, 2024.